Sana'a University Journal of Applied Sciences and Technology https://journals.su.edu.ye/index.php/jast
Vol. 1 | No. 3 | Page 253 – 265 | 2023 | ISSN : 2958-9568
Doi: 10.59628/jast.v1i3.522

Localized Plastic Deformation and Microstructure Properties of Al/Si Alloy Improved with Al_3Ni Compound

Shakib Alsowidy [1,*], Belqueis Al-Asry [1,*], Olfat Humaid [1,2]
[1] Physics Department, Faculty of Science, Sana 'a University, Yemen.
[2] Physics Department, Faculty of Science, Hajjah University, Yemen.
***Corresponding author** : *sh.alsowidy@su.edu.ye and alasryb@gmail.com*

ARTICLE INFO
Article history:
Received: July 15, 2023
Accepted: July 25, 2023
Published: August, 2023

KEYWORDS
1. Hypoeutectic
2. Vickers Hardness
3. Al/Si
4. Microstructure
5. Mismatch
6. Modified
7. XRD

ABSTRACT
The microstructure of AS10/xNi hypoeutectic alloys with (x = 0.01% and 0.05%) was investigated using X-ray diffraction (XRD) and scanning electron microscopy (SEM). Localized permanent plastic deformation (Vickers hardness (HV)) was conducted on the samples before and after sintering. After sintering, the results showed a significant improvement in hardness with the addition of Ni atoms. From the XRD map, it was found that there was a shift in the peak positions as the Ni atoms were added. This shift is a result of the in coincidence of d_{hkl} levels in the Al-phase before and after the addition of Ni. This mismatch in d_{hkl} levels is associated with the lattice defects and lattice parameters. From the SEM images, the silicon powder particles in the binary composition are large and elongated plates, whereas those in the ternary composition are small and semi-spherical particles. This reduction in the particle size of the modified alloy is attributed to the presence of Ni atoms in the alloys.

CONTENTS

1. Introduction:

Aluminum is widely used when low weight and low cost are required. Therefore, high-content aluminum alloys are widely used as structural materials.

To withstand severe operating conditions, structural materials in the automotive industry are made of cast iron and its alloys. Aluminum and its alloys are considered the lightest structural metals available.

Owing to modern structural industries requiring strong and lightweight metals and growing desire to minimize fuel consumption, these requirements are very important to the economy and are environmentally-friendly and must be taken into account.

Currently, aluminum and its alloys are the most widely used light metals. The advantages of Al

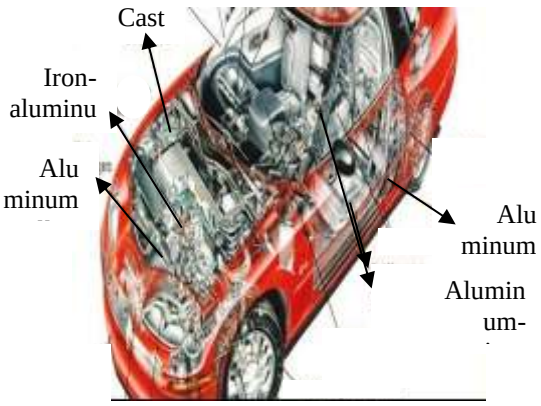

Figure 1: The car body is made of lightweight aluminum alloy

include a low density about 2.7g/cm3 and high plastic deformation of up to 30 percent

Aluminum alloys, such as Al/Si, Al/Mg, and Al/Cu, have various Characteristics such as resistance to corrosion, mechanical strength, good castability, ability to work at RT up to 400 °C, responsiveness to heat treatment, and low cost.

Their high strength-to-weight ratio (~150-180 Mpa/kg) makes them an appropriate alternative for applications that require weight savings.

Currently, the components of the automotive industry, particularly electric vehicles and internal combustion vehicles, are mostly made of Al and its alloys (Figure 1).

All alloys mentioned above have an α-Al dendrite phase. The spacing between dendrites is an important factor in determining the alloy properties, such as the strength of the alloy.

As the spacing between the main and secondary dendrites decreases, the structure becomes finer [1].

The addition of an alloying element to the Al major produces secondary phases, especially intermetallic compound phases, that reduce the secondary dendrite arm spacing (SDAS) and then refine the microstructure [2].

Heat treatment of metal at various temperatures is considered a favorable technique for enhancing the characteristics of aluminum after casting and cold working [3].

Aluminum–Silicon alloys are commonly subjected to a variety of mechanical loads and relatively harsh environmental conditions when employed in structural applications. These stresses can cause long-term irreversible plastic deformation before failure, even if they are below the yield strength of the aluminum alloys. As a structural material, it has a high resistance to ambient environmental stresses as its service life has improved. It is generally known that localized plastic deformation and mechanical plastic strain decrease as the number of microstructure defects increases [4]. However, in addition to the possibility of high dislocation concentrations in pure aluminum that may be produced after cold-working, pure Al has significantly poor mechanical properties, such as low hardness (~20 HB) and low yield strength (~70 MPa) [5]. The poor mechanical properties of this material are a result of microstructural defects. To address these issues, the density of defects across the dendritic microstructure must be dramatically reduced. To increase its mechanical strength and reliability, the current study is an attempt to improve the microstructural characteristics of the AS10 alloy by adding traces of nickel alloying elements.

2. Materials and Methods

The nanopowders aluminum, silicon, and nickel were accurately weighed in balance to obtain the required composition, as shown in Table (1) with a purity of 99.99% for all elements. The balanced elements were mixed in powder form at room temperature. The balanced powder mixture was subjected to compression using a hydraulic pressure system with a constant load of 250KN for 5 min for all the three samples. Compacted circular disks with dimensions of 6×32 mm are shown in Figure (2). Subsequently, the compressed samples were sintered in a

controlled-atmosphere furnace at approximately 773 K to allow the particles to bind to each other.

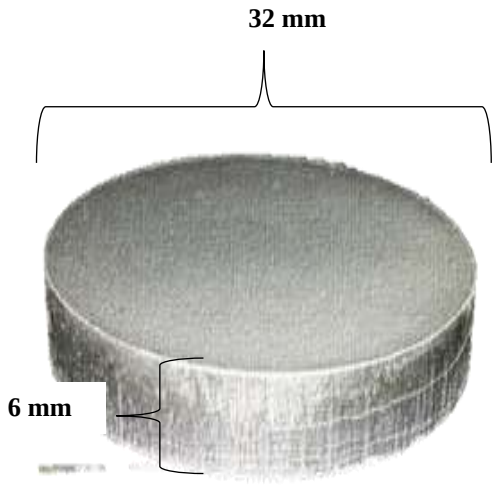

Figure 2: Compressed Sample

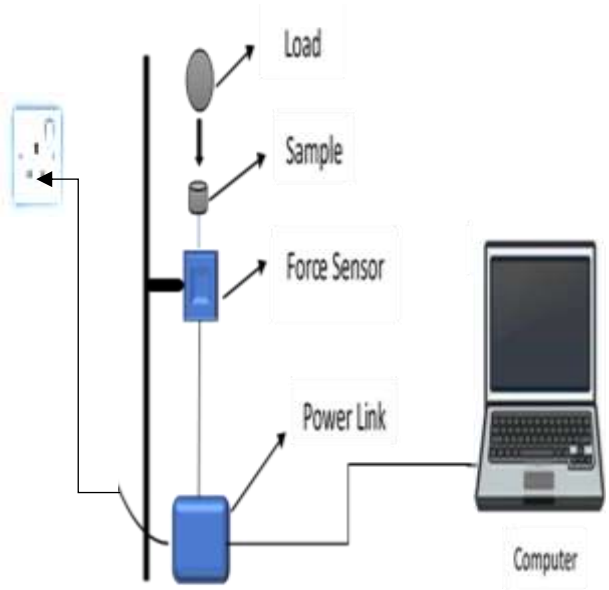

Figure 3: Schematic diagram of Vickers hardness tester

A Vickers hardness test (localized plastic deformation resistance or impact force resistance) was performed using mechanical equipment, as shown in Figure (3).

The microstructures of the samples were investigated using X-ray diffraction and scanning electron microscope techniques. The SEM imaging was performed by irradiating the samples with a highly accelerated electron beam.

Secondary electrons (SE) and backscattered electrons (BSE) produced from the top and bottom of the samples were detected and processed by a scanning backscattered electron detector (SBED) and finally displayed as an image on the screen.

Table 1 : Chemical composition of the Al-Si–Ni alloys

Alloy	Sample	Si	Ni	Al
AS10	A_0	10%	0	Balance
AS10-0.01Ni	A_1	10%	0.01%	Balance
AS10-0.05Ni	A_2	10%	0.05%	Balance

2.1. Vickers Hardness

In Vickers hardness testing, pyramidal indenter methods are used to produce geometrically identical indentations [6]. At least three indentations were made for each specimen, and the average of these indentations served as the representative hardness value. The Vickers hardness number (HV) was calculated using the following expression [7]:

$$HV = 1.85\frac{L}{d^2} \qquad (1)$$

where L is the indentation load (kg) and d is the mean diagonal of the indentation in mm.

2.2. X-ray Diffraction

X-ray diffraction is a common analytical technique used for phase identification. This technique is based on the elastic scattering of X-rays from crystal structures to produce diffraction patterns. Subsequently, the diffraction pattern was used to index the crystallographic structure of the phases of the material.

Phase identification of the alloy samples was carried out using X-ray diffraction to analyze and

observe the variation of the microstructure with the concentration of Ni atoms. An X-ray Shimadzu EDX-720 model with Cuk$_\alpha$ radiation (λ =1.54056) and a diffraction angle 2θ ranging from 5° to 75° was used.
The source was operated at an accelerating voltage of 40 kV and a tube current of 20 mA. Continuous scanning was performed at a constant scanning rate of 0.02 sec^{-1}. Particle size (D) was calculated using the Scherrer equation:

$$D = \frac{0.9\,\lambda}{\beta \cos\theta} \qquad (2)$$

, where β is the broadening of the diffraction line, which is the full width at half maximum of the peak, θ is the diffraction angle, and λ is the X-ray wavelength. The dislocation density (δ) was calculated using the following equation:

$$\delta = \frac{1}{D^2} \qquad (3)$$

2.3. Scanning Electronic Microscopy

The microstructures of the samples were analyzed using scanning electron microscopy (SEM) (JEOL JSM 6510 Lv) at Mansoura University, Egypt. The microscope operated at an accelerating voltage of 5–30 kV and had an energy dispersive spectroscopy (EDS) facility. The SEM employed in this investigation had operational modes for energy-dispersive X-ray spectroscopy (EDS), secondary electron imaging, and primary electron imaging. SEM provides high-quality images at high magnification because it has a deeper field of view and greater resolution than optical microscopy (up to 50,000 ×).

3. Results and Discussion

3.1. Vickers hardness measurements

Table 2: lists the Vickers hardness values of AS10-xNi specimens before and after sintering. The hardness increases from 62.6 to 78.9 at 0.01% Ni and also from 67 to 86.9 at 0.05% Ni. From Table 2, the highest hardness value at 0.05% Ni before sintering is 67.37 HV, while the highest hardness value at 0.05% Ni after sintering is 86.98 HV.

From the Vickers hardness results, it was found that by increasing the Ni-content, HV significantly increased before and after sintering, as shown in Figure 4.
From the Al/Ni-binary phase diagram, it is clear that the maximum solubility of Ni in Al is 0.04%, and most Ni constituent atoms react with Al atoms to produce Al_3Ni chemical compounds. By increasing the Ni-content, the amount of Al_3Ni increased, as observed in the SEM images. The formation of a hard Al_3Ni-IMC improves the mechanical strength, which is a very important characteristic of automotive Al-alloys [8, 9].
Table 2 :Vickers Hardness Number (VHN) for Alloys

Material	Vickers Hardness (HV) Before Sintering	After Sintering
A_0	56.01	59
A_1	62.66	78.95
A_2	67.37	86.98

In the literature [10,11] and in ceramic materials, Al_3Ni chemical compound has a complex crystal structure (orthorhombic), and works as a dislocation slip resistance.

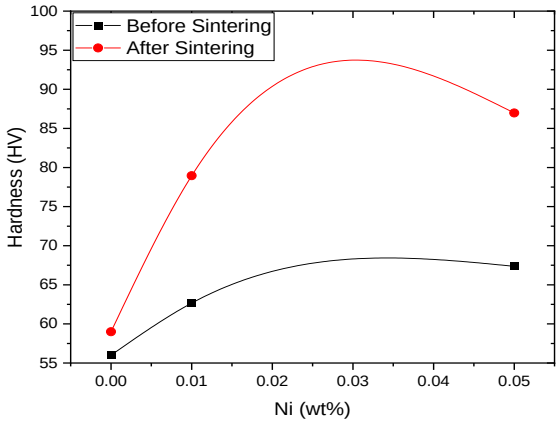

Figure 4: VH as a function of Ni -content

Therefore, the dislocation slip was destroyed, and the material became hard. All these factors

make the Al alloy stronger and result in a higher surface indentation resistance.

3.2. XRD analysis

XRD is a popular characterization technique for identifying the phases present in metal alloys. A structural study utilizing X-ray diffraction was performed to identify the different phases in the alloys. The original XRD-patterns for all compacted samples are shown in Figure 5.

The obtained diffraction patterns were compared with the standard powder diffraction data (PDF) using a search/match process of measured data with appropriate reference file using jade6.5 software. These patterns show the variation in the diffracted beam intensity with Bragg's angle, and some sharp peaks are clearly observed. This observation confirmed the polycrystalline nature of the samples examined. These peaks were reflected in the number of phases and crystallinity. Three large peaks represent the Al-phase with lines of (111), (200), and (220), and four small peaks for the Si-phase with the (111), (220), (311), and (400) lines. This is shown in more detail in Tables (3a) and (3b).

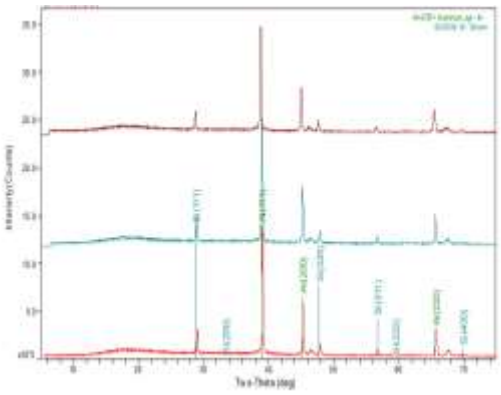

Figure 5: XRD pattern for AS10-xNi

Table 3b: Intensity of Si lines for all samples

Lines	Intensity		
	A_0	A_{100}	A_{500}
Si (111)	1905	1889	1324
Si (200)	1046	1073	814
Si (220)	723	471	489
Si (400)	105	122	82

Table 4: Crystal systems and (JCPDS-ICDD) references of AS10 alloy systems

Sample in wt%	Phases	Crystal system	(JCPDS-ICDD) Reference
A_0	Al	Face centered cubic (FCC)	PDF#04-0787
	Si		PDF#80-0018
A_{100}	Al	Face centered cubic (FCC)	PDF#04-0787
	Si		PDF#80-0018
A_{500}	Al	Face centered cubic (FCC)	PDF#04-0787
	Si		PDF#80-0018

The phases and crystal systems are shown in Figure 5: are summarized in Table (4) and compared with the references of the Joint Committee on Powder Diffraction Standards (JCPDS) at the International Center for Diffraction Data (ICDD). A comparison of the patterns before and after Ni-addition reveals the following: (i) the Al peak intensity changed after Ni-addition, especially for the Al (111) line. This intensity decreased with an increase in the Ni content. This is the first evidence of a reduction in the amount of Al-phase. This may be due to a chemical reaction between the Al and Ni atoms. According to the S/M process, previous literature [12], and the Al-Ni phase diagram [13], this chemical compound is Al_3Ni orthorhombic. This phase was not observed in the XRD patterns because its amount was too small for detection (Table 1). To verify the existence of the chemical compound phase, the S/M process was performed twice for each sample before and after removing the background, as shown in Figure 6a and 6b, respectively. (ii) There was a shift in the peak positions with the addition of Ni atoms. This shift shifted to the left and increased with increasing Ni-content, as shown in Figure 7 and Tables 5a and 5b. This shift is a result of the incoincidence of d_{hkl} levels before and after the addition of Ni to the Al-phase. This inconsistency in d_{hkl} levels is associated with lattice defects and changes in the lattice parameters, as shown in Tables 6a and 6b. The Al atoms were slightly below their original positions. This may be due to the sintering process, which promotes the diffusion and spreading of Ni atoms in Al-cells.

This process is called an interstitial solid solution of Ni atoms in Al cells. From the previous observations, it can be concluded that Ni addition causes a small microstrain in the Al and Si lattices and produces the Al_3Ni chemical compound.

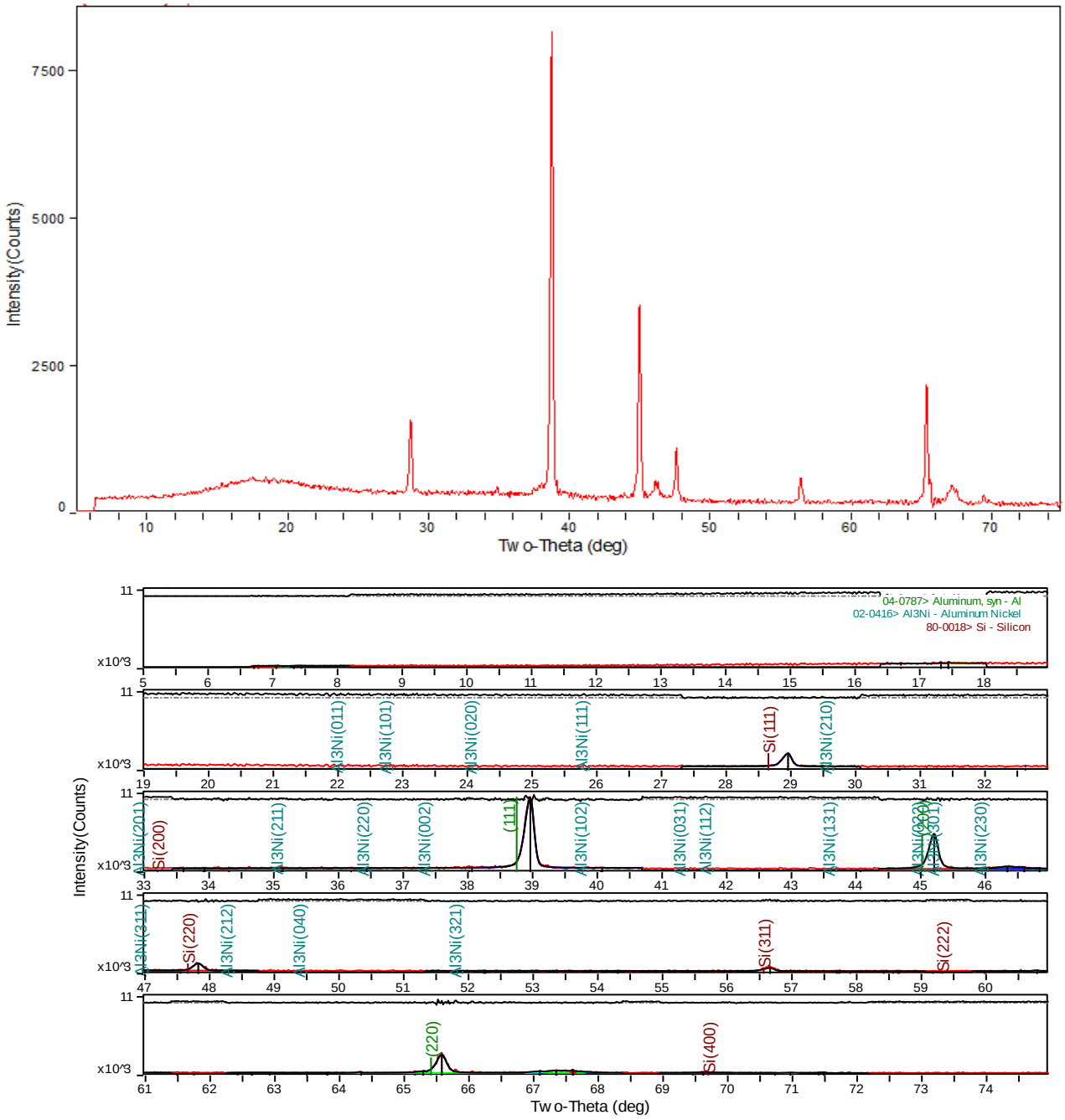

Figure 6a: XRD patterns for AS10-0.01Ni without and with background

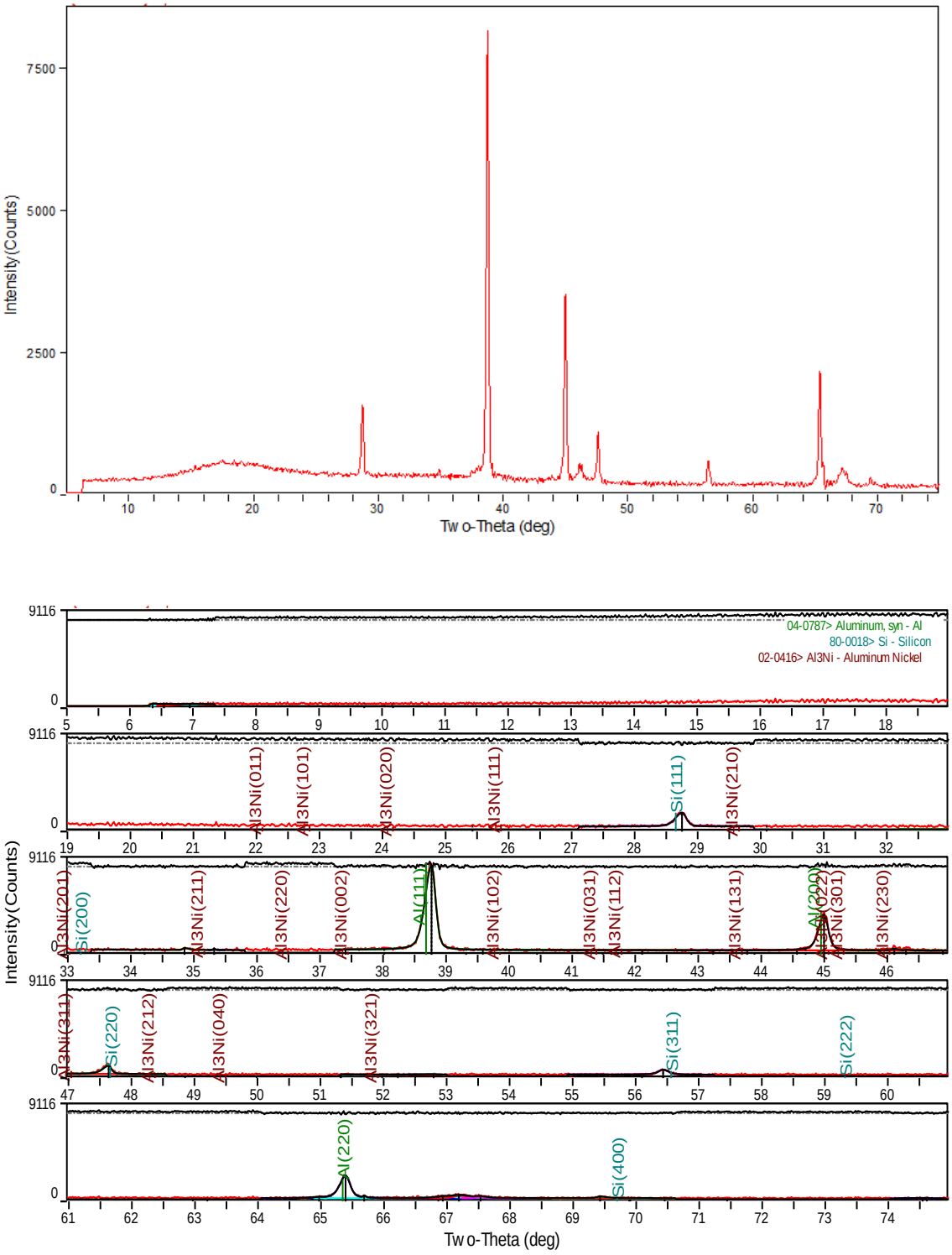

Figure 6b: XRD patterns for AS10-0.05Ni without and with background

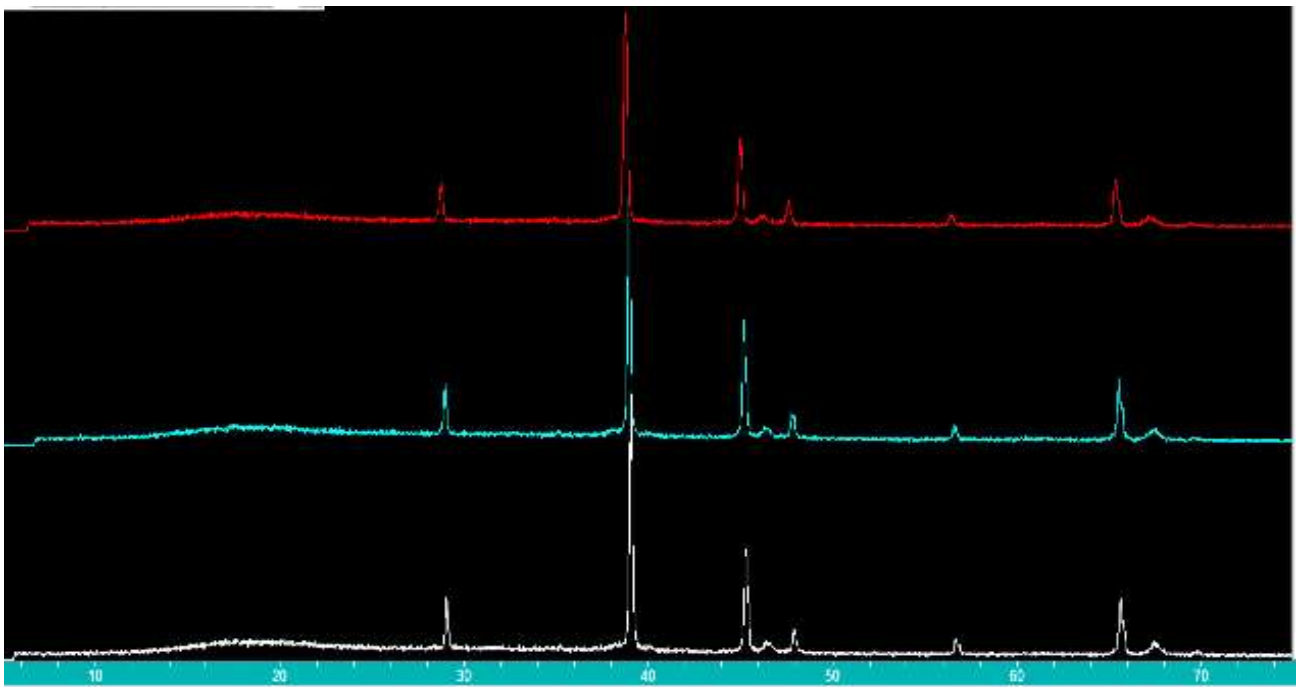

Figure 7: Magnified XRD pattern of AS10-xNi from Jade program

Table 5a: The angle of Al lines for all samples

Lines	Lattice constant (A^0)		
	A_0	A_{100}	A_{500}
Al (111)	3.991	4.000	4.019
Al (200)	3.999	4.008	4.025
Al (220)	4.017	4.022	4.033

Table 5b: The angle of Si lines for all samples

Lines	2 Θ (Degree)		
	A_0	A_{100}	A_{500}
Si (111)	29.048	28.957	28.752
Si (220)	47.906	47.826	47.64
Si (311)	56.692	56.663	56.436
Si (400)	69.864	69.699	69.888

Table 6a: lattice constant of Al lines for all samples

Lines	Lattice constant (A^0)		
	A_0	A_{100}	A_{500}
Al (111)	3.991	4.000	4.019
Al (200)	3.999	4.008	4.025
Al (220)	4.017	4.022	4.033

Table 6b: lattice constant of Si lines for all samples

Lines	Lattice constant (A^0)		
	A_0	A_{100}	A_{500}
Si (111)	5.319	5.336	5.373
Si (220)	5.366	5.374	5.394
Si (311)	5.380	5.383	5.403

3.2.1 Particle size and dislocation density

According to Scherrer formula (2), The particle size (D) of the AS10-xNi alloys was determined according to the Scherrer formula (2) and is displayed in Table 7. Table 7 shows that the addition of Ni slightly reduced the average particle size of the AS10-xNi alloy. Particle size reduction may be attributed to the presence of Al_3Ni-IMC in alloys, which acts as a barrier to Al and Si growth through slow cooling after the sintering process, resulting in particle size reduction. The variation in the average particle size was computed and plotted against the Ni content, as shown in Figure 8.

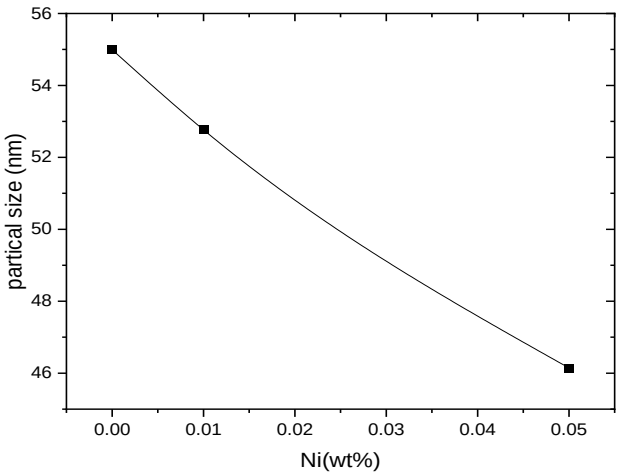

Figure 8: The variation in particle size values of Al with Ni-content

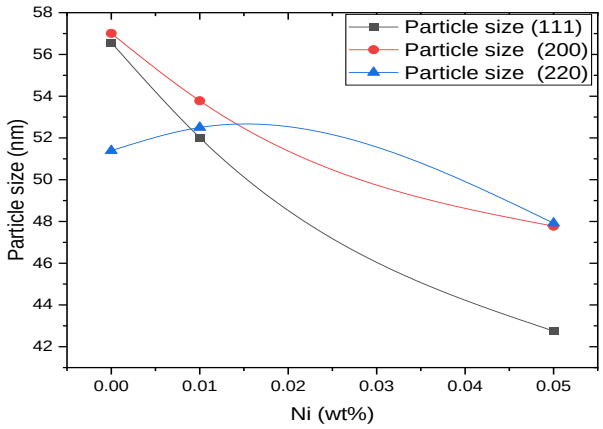

Figure 9: The variation in particle sizevalues of crystallographic direction inAS10 with Ni-content

Table 7: Particle size and dislocation densityof Al-Si-xNi alloys

Samples	Line	Particle Size (nm)	dislocations Density (nm^{-2}) *10^-5
Al-10Si	111	56.571	33
	200	57.009	
	220	51.389	
Al - 10Si-0.01%Ni	111	52.017	36
	200	53.783	
	220	52.500	
Al - 10Si-0.05% Ni	111	42.749	47
	200	47.770	
	220	47.918	

According to Fig. (9), the Ni concentration affects the particle size for all lines. In general, the particle size decreases for each line with an increase in the nickel content. Poisson's ratio provides a significant interpretation of this behavior of particle size with various orientations (111), (200), and (220). Poisson's ratio is the ratio of transverse strain to the equivalent axial strain on a material under axial stress [14].

To study the defects in the density of the AS10-xNi alloys, the dislocation density (δ) was calculated using Equation (3), and plotted as a function of the Ni-content, as shown in Table 7 and Figure 10. It is evident from this Figure and Table 7 that there is an increase in the dislocation density values as more Ni is added. This may be a result of a reduction in particle size, which further restricts the movement of dislocations and improves creep resistance. The increasing dislocation density is considered to be an indication of the enhancement in the mechanical strength of the alloy.

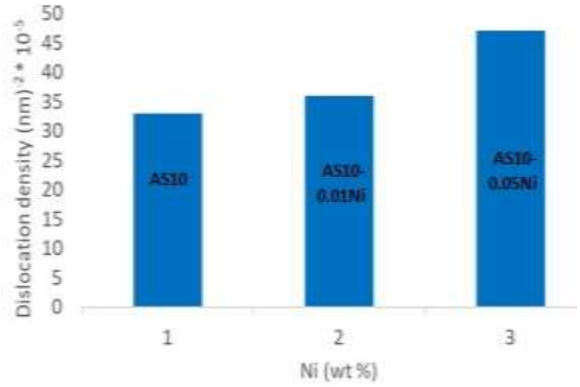

Figure 10: Variation in dislocation density values with Ni-content

3.4 Scanning electron microscope

In order to investigate the microstructure and the effects of Ni addition on the characteristics of the Al-Si alloy, the morphology

and topography of unmodified and modified specimens were examined using secondary electron (SE) and backscattered electron (BSE) images produced by scanning electron microscopy, as shown in Figure 11.

It is well known, that the microstructure of Al/Si/Ni contains many different phases and has a finer structure than that containing only one or two phases [15]. This phenomenon was expected and was detected in this work when modifying the Al/Si binary composition by adding traces of Ni-atoms into the Al/Si binary. These changes in microstructure size are clear when comparing Figures (11a and 11b, c,). In Figure 11 , it can be observed that there are three regions in the overall structure. The first region is the large elementary Al powder particles with a black-gray color. The second region is the master alloy, which consists of primary silicon surrounded by the third region of the eutectic Al-Si structure (white grey).

As the force increased gradually during compaction, the nanocomposite structure began to produce a sandwich structure. (12a). This occurred because of the collision of the particles during compaction. During sintering, this structure facilitates the welding of the particles together and produces rough surfaces with coarse grains (large size), as shown in Fig. (12b). The successive welding of the particles continued because of the sintering treatment. This leads to the formation of a dense structure and a higher hardness. It can be seen that the primary Si is independent of the Al-Si alloy. Cracked silicon particles can be observed in many regions. This observation may be due to the indentation region that occurred during testing. In the unmodified and modified alloys, many pores were uniformly distributed in the overall structure.

If one compares the binary and ternary alloys from Figures (13a) and (13b,c), respectively, they will detect that in the binary composition, the particles are in the form of elongated plates with large sizes, whereas they are small elongated plates and semi-spherical particles in the ternary composition. This reduction in the size of the modified alloy was attributed to the presence of millions of Ni atoms added to the alloys. From the AL/Ni binary equilibrium phase-diagram, Al and Ni atoms engaged in a chemical reaction, and from the Al_3Ni IM'C-phase. It can be observed that Al_3Ni was included in the structure as small black particles distributed randomly in the microstructure, as shown in Fig.(13c). The key factor behind HV improvement is this new phase. Similar to ceramic materials, any chemical compound works as a dislocation slip resistance; therefore, the dislocation slip is destroyed and the material becomes harder

[15,16]. These factors resist the indentation of the Al surface.

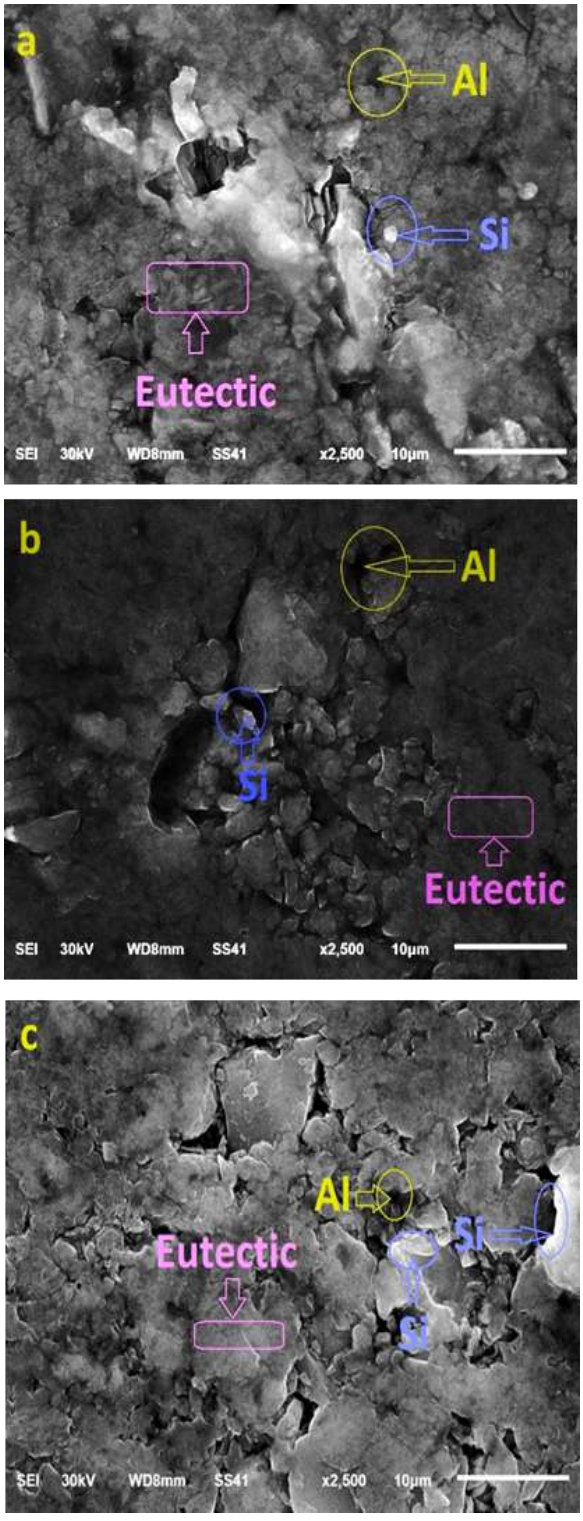

Figure 11: SEM images of the a) hypo-eutectic AS10, b) Ni added (100ppm), c) Ni added (500ppm)

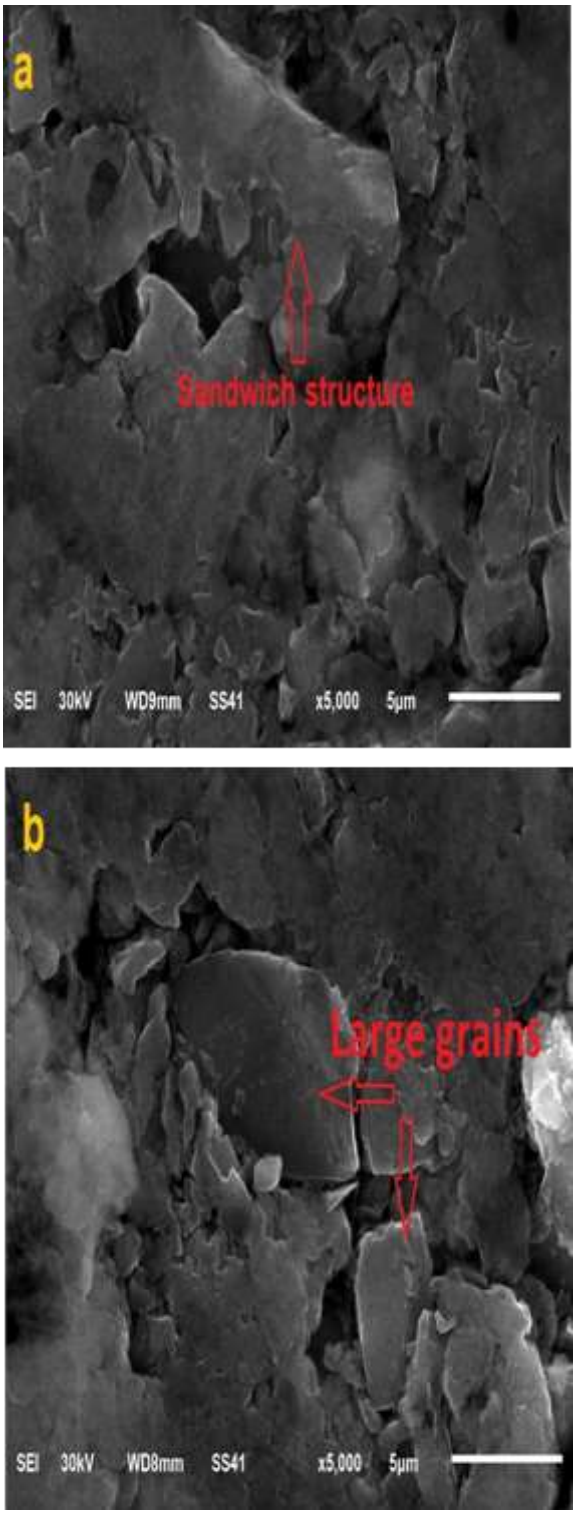

Figure 12: Different grain shapes due to compaction and sintering

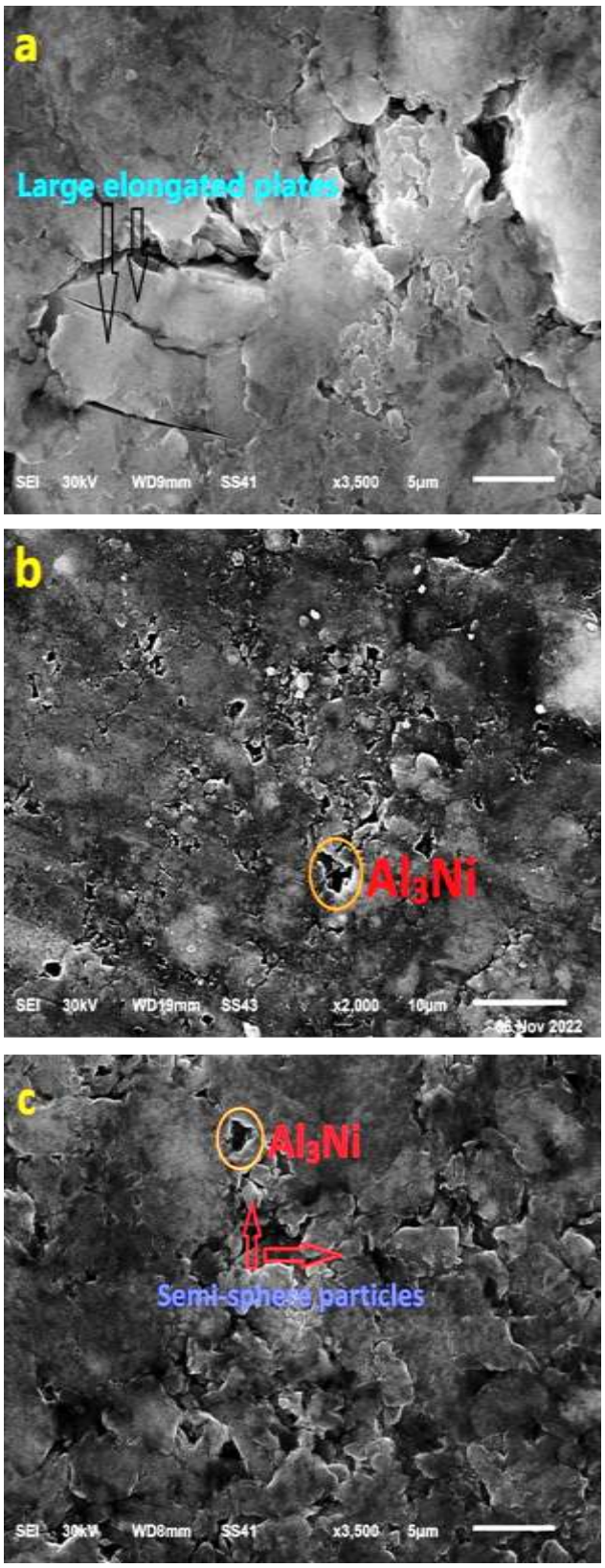

Figure 13 : (a)Binary and (b,c)ternary alloys form

4. Conclusion

In this study, the Vickers hardness and microstructure of Al/10wt%Si-100 ppm Ni and Al-10wt%Si-500 ppm Ni were investigated.
The results are summarized as follows.
1 -The ternary alloy has a higher localized plastic deformation (hardness) value than the binary one due to the formation of the chemical compound of Al_3Ni.
2 -The Al peak's intensity decreases as the Ni amount increases.
3 - From the SEM images, it can be concluded that the silicon powder particles in the ternary composition were smaller and semi-spherical. The addition of Ni atoms to the alloys may be responsible for the reduction in the size of the modified alloy structure.
4-When increasing Ni-content the dislocation density increased. This might be due to a decrease in the particle size, which further constrained the dislocation movement and enhanced the creep resistance.
5- The formation of Al_3Ni IMC in the microstructure of Al/10Si and the increase in its volume fraction with Ni-content are considered to be the main reasons for the enhancement in hardness and microstructure properties.

5. References

[1] M. Gandolfi, M. G. C. Xavier, L. F. Gomes, R. A. V. Reyes, A. Garcia, and J. E. Spinelli, "Relationship between microstructure evolution and tensile properties of alsi10mg alloys with varying mg content and solidification cooling rates," Metals (Basel)., vol. 11, no. 7, pp. 1–23, doi: 10.3390/met11071019,2021. https://www.mdpi.com/2075 4701/11/7/1019

[2] A. Chaus, E. Marukovich, and M. Sahul, "Effect of rapid quenching on the solidification microstructure, tensile properties and fracture of secondary hypereutectic al-18%si-2%cu alloy," Metals (Basel)., vol. 10, no. 6, pp. 1–13, doi: 10.3390/met10060819,2020. https://www.mdpi.com/2075-4701/10/6/819

[3] A. Manente and G. Timelli, “Optimizing the Heat Treatment Process of Cast Aluminium Alloys,” 2002. https://www.intechopen.com/chapters/24039

[4] R. Sitek et al., “The Impact of Plastic Deformation on the Microstructure and Tensile Strength of Haynes 282 Nickel Superalloy Produced by DMLS and Casting,” Materials (Basel)., vol. 15, no. 21, doi: 10.3390/ma15217545, 2022. https://www.mdpi.com/1996-1944/15/21/7545

[5] A. Mostafa؛ W. Adaileh؛ A. Awad, and A. Kilani, “Mechanical Properties of Commercial Purity Aluminum Modified by Zirconium Micro-Additives,” pp. 1–14, 2021. https://www.mdpi.com/2073-4352/11/3/270

[6] M. Tiryakioğlu؛ J. S. Robinson؛ M. A. Salazar-Guapuriche؛ Y. Y. Zhao, and P. D. Eason, “Hardness-strength relationships in the aluminum alloy 7010,” Mater. Sci. Eng. A, vol. 631, pp. 196–200, doi: 10.1016/j.msea.2015.02.049, 2015. https://www.sciencedirect.com/science/article/abs/pii/S0921509315001665

[7] Krishna.S and Karthik.M, “Evaluation of Hardness Strength of Aluminium Alloy (AA6061) Reinforced With Silicon Carbide,” Int. J. Recent Technol. Mech. Electr. Eng., vol. 1, no. 4, pp. 14–18, 2014, [Online]. Available: http://www.ijrmee.org/download/1428305064.pdf

[8] J. R. Davis, Aluminum and aluminum alloys. ASM international, 1993. https://materialsdata.nist.gov/bitstream/handle/11115/173/

[9] J. Grandfield؛ L. Sweet؛ A. Beer؛ S. Zhu؛ X. Chen, and M. Easton, “The Effect of Trace Levels of Ni and V on the Microstructure and Properties of Four Common Aluminum Alloys,” Light Met. 2014, vol. 9781118889, pp. 969–974, doi:10.1002/9781118888438.ch161, 2014. https://link.springer.com/chapter/10.1007/978-3-319-48144-9_161

[10] T. Bogdanoff, “Development of aluminium-silicon alloys with improved properties at elevated temperature,” Mater. Manuf., no. May, p. 4, [Online], 2017. Available: http://urn.kb.se/resolve?urn=urn:nbn:se:hj:diva37499%0Ahttps://drive.google.com/open?id=0B0fTxDBXtHZMTFltNXlSc29KUTA

[11] J. Silvestre؛ N. Silvestre, and J. De Brito, “An overview on the improvement of mechanical properties of ceramics nanocomposites,” J. Nanomater., vol. 2015, 2015, doi:10.1155/2015/106494. https://www.hindawi.com/journals/jnm/2015/106494/

[12] M. Farag؛ M. Kh, A. Atlam, and A. Omran, “Characterization of Al-Si-Ni Ternary Alloy Synthesis From Reduction of Sodium-Fluosilicate and Nickel Oxide,” J. Al-Azhar Univ. Eng. Sect., vol. 13, no. 48, pp. 1100–1108, 2018, doi: 10.21608/auej. 18989,2018.. https://journals.ekb.eg/article_18989.html

[13] K. Hilpert et al., “Phase Diagram Studies on the Al-Ni System,” Zeitschrift fur Naturforsch. - Sect. A J. Phys. Sci., vol. 42, no. 11, pp. 1327–1332, 1987, doi: 10.1515/zna-1987-1117. https://www.altstu.ru/media/f/Dissertaciya-Trung.pdf

[14] H. Ford, Materials science and engineering, vol. 14, no. 1. 1974. https://anupturnedworld.files.wordpress.com/2016/06/callister-materials-science-and-engineering.pdf

[15] M. S. Kaiser؛ S. H. Sabbir؛ M. S. Kabir؛ M. R. Soummo, and M. Al Nur, “Study of mechanical and wear behaviour of hyper-eutectic Al-Si automotive alloy through Fe, Ni and Cr addition,” Mater. Res., vol. 21, no. 4, 2018, doi:10.1590/1980-5373-MR-2017-1096. https://www.scielo.br/j/mr/a/kkcQhyJknMx9vQYM3yMpF3k/?format=html&lang=en

[16] M. Sudmanns and J. A. El-Awady, “The effect of local chemical ordering on dislocation activity in multi-principle element alloys: A three-dimensional discrete dislocation dynamics study,” Acta Mater., vol. 220, 2021, doi: 10.1016/j.actamat.2021.117307. https://www.sciencedirect.com/science/article/abs/pii/S135964542100687X

[17] T. E. Mitchell, “Dislocations in Ceramics,” Ceram. Sci. Technol., vol. 2–4, no. November 1985, pp. 379–436, 2013, doi: 10.1002/9783527631940.ch21. https://www.tandfonline.com/doi/abs/10.1179/mst.1985.1.11.944